15th Canadian Masonry Symposium
Ottawa, Canada
June 2-5, 2025

Numerical Analysis of TPMS Masonry Assemblages

Fahimeh Yavartanoo[i] and Damon Bolhassani[ii]

ABSTRACT

Masonry structures have been used in construction for centuries due to their durability, ease of maintenance, and availability of materials. However, in recent years, with the rising costs of labor and the pressures of conserving natural resources, which have led to a scarcity of traditional materials, masonry has lost its edge against steel and concrete. Moreover, traditional unreinforced masonry structures are often considered vulnerable under seismic conditions due to their brittle nature and high mass. While these concerns have influenced design preferences in some regions, modern innovations such as reinforced or confined masonry have demonstrated improved seismic performance and remain widely adopted. This study aims to further advance masonry design by exploring lightweight, structurally optimized units using the Triply Periodic Minimal Surface (TPMS) approach. This method reduces material usage while maximizing surface coverage, enhancing sustainability, and providing high structural strength, making them highly cost-effective. Their lightweight nature also facilitates easier transportation and handling, reducing labor demands. Furthermore, their unique and visually appealing design allows for use as combined structural and non-structural elements or as architectural elements such as decorative walls or facades. First, three TPMS units, P.Schwarz, Gyroid, and Hybrid, were designed, and their performance was evaluated experimentally and numerically. All TPMS units showed good mechanical performance under compression, though Gyroid was superior to P. Schwartz, and Hybrid had the higher resistance among them. Then, by applying Finite element (FE) models developed in ABAQUS, two types of assemblages were designed using TPMS units to investigate the behavior of prisms and diagonal tension assemblages to compressive load.

KEYWORDS

TPMS units, Minimal surface, Masonry structures, Finite element models, ABAQUS.

[i] Postdoctoral researcher, ABC LAB, The City College of New York (CCNY), New York, USA, fyavartanoo@ccny.cuny.edu
[ii] Assistant Professor, The City College of New York (CCNY), New York, USA, mbolhassani@ccny.cuny.edu

INTRODUCTION

Masonry has been a fundamental element of architectural construction for thousands of years, valued for its durability, load-bearing capacity, and availability of raw materials. From ancient monuments to modern buildings, it has played a central role in architectural advancements. However, despite its historical significance, traditional masonry faces several challenges in contemporary construction. Rising labor costs and material scarcity have impacted its competitiveness compared to steel and concrete. Additionally, while conventional unreinforced masonry has shown vulnerability during seismic events, modern solutions such as reinforced or confined masonry have significantly improved resilience and remain broadly accepted in earthquake-prone regions (Bolhassani and Wisniewski, 2022; Nazir et al., 2021; Ferdous et al., 2019; Yavartanoo et al., 2024). These developments underscore the importance of continuing to enhance masonry systems through innovative geometries and sustainable materials. Additionally, the environmental impact of masonry materials, such as cement-based products, has raised sustainability concerns, driving the demand for more eco-friendly alternatives. In response to these challenges, researchers have developed geometrically optimized systems that utilize computational design and additive manufacturing technologies (Van Mele et al., 2012). Among these innovations, Triply Periodic Minimal Surfaces (TPMS) have emerged as a groundbreaking approach to sustainable and functional design. TPMS geometries are defined by smooth, continuous surfaces with periodic repetitions that optimize material usage while achieving high strength-to-weight ratios and energy absorption capabilities (Qiu et al., 2024; Feng et al., 2022; Meza et al., 2014). These geometries not only reduce material consumption but also improve mechanical performance, making them ideal for architectural applications such as facades, non-load-bearing partitions, and decorative walls. Their porous structures and lightweight designs enable modular assembly, while their complex geometries accommodate vegetation, making them suitable for green walls that support urban sustainability. In addition, their open-cell structures make them particularly useful for marine applications, such as coral reef restoration, by providing voids for marine habitats while maintaining structural integrity in aquatic environments (Nguyen-Van et al., 2020; Sokollu et al., 2022; Yoris-Nobile et al., 2023). Recent numerical and experimental studies have further validated the viability of TPMS-based structures under compressive and tensile loads, revealing their ability to evenly distribute stress and optimize deformation patterns (Hooshmand-Ahoor et al., 2024). Through Finite Element (FE) modeling, researchers have successfully simulated the mechanical behavior of these geometries under compressive forces, confirming their strength, resilience, and practical applications (Gide and Bagheri, 2024). These studies highlight the potential of TPMS systems to address the limitations of traditional masonry while offering aesthetic appeal, sustainability, and structural efficiency. Building on these findings, this study explores the application of TPMS units by developing FE models to design and analyze two types of assemblages: prisms and diagonal tension assemblages. These configurations were subjected to compressive loads to investigate their mechanical behavior and structural performance. First, three TPMS geometries, P.Schwarz, Gyroid, and Hybrid, were fabricated, tested, and analyzed experimentally and numerically. Therefore, initial evaluations focused on unit-level performance, employing Concrete Damaged Plasticity (CDP) modeling in ABAQUS to simulate nonlinear material behavior under compressive loads. These tests revealed promising results, particularly for Hybrid designs, which exhibited enhanced load-bearing capacity and deformation resistance. The detailed methodology and results of these tests were comprehensively presented in our previous study (Righi et al., 2024). Then, the same methodology was used for a total of 6 models, including two different assemblages, using three TPMS units. The results of this study allowed for a detailed examination of stress distributions, deformation patterns, and failure modes within the assemblages, providing valuable insights into the interaction between the units and the overall assembly.

Numerical Modeling Process

This paper focuses on the numerical modeling of TPMS assemblages; however, to provide essential background information on the individual TPMS units, this section briefly summarizes the experimental and numerical testing of these units under compressive loading.

Calibration and Validation of TPMS Units

The experimental study focused on the fabrication and mechanical testing of three distinct TPMS geometries, P. Schwarz, Gyroid, and Hybrid, to evaluate their load-bearing capacity, failure modes, and stress distribution (Fig. 1a and b). A high-strength self-consolidating concrete mixture was utilized for casting the units, incorporating silica fume, superplasticizer, and microfibers to enhance strength, workability, and crack resistance. The specimens were cured for 28 days before testing. A universal testing machine (UTM) with a capacity of 2224.11 kN was used to apply compressive loads incrementally. The tests revealed significant differences in performance among the geometries. The P. Schwarz specimen failed at 7.19 kN, exhibiting tensile-dominated failure initiated by stress concentrations and circumferential deformation due to its high curvature and reduced effective area. The Gyroid specimen, with a more efficient geometry for load distribution, demonstrated superior performance, failing at 18.52 kN, approximately 2.5 times higher than the P. Schwarz model. The Hybrid specimen outperformed both, sustaining a load of 88.38 kN, about 12 times that of P. Schwarz and 5 times that of Gyroid due to its optimized geometry, which minimized stress concentrations and provided better material utilization.

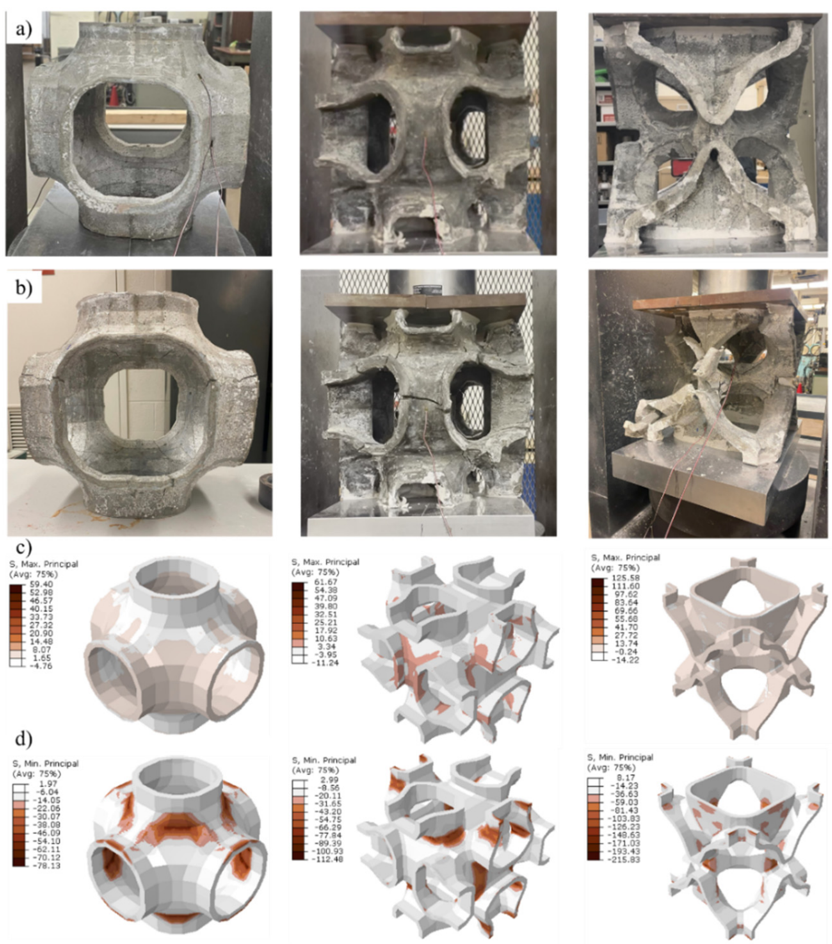

Figure 1: a) TPMS units; b) Fracture mechanism; c) Principle tensile stress; and d) Principal compressive stress

The numerical analysis was conducted using finite element modeling (FEM) in ABAQUS, employing the Concrete Damage Plasticity (CDP) model to simulate the nonlinear behavior of the TPMS concrete units under compressive loading. The models were discretized using C3D10 tetrahedral elements with a mesh size of 10 mm to accurately capture stress variations. Rigid steel plates were modeled at the top and bottom surfaces of each specimen, and tie constraints were used to ensure perfect bonding between the plates and the concrete units. A displacement-controlled loading approach was applied to the top plate, and a static general solution scheme with nonlinear geometry was activated to account for large deformations during loading. The numerical results closely matched the experimental findings, with stress concentrations and failure patterns predicted in the finite element analysis (FEA) aligning well with the cracks observed in the physical tests (Fig. 1b and c). For the P. Schwarz specimen, numerical predictions indicated stress localization at the mid-height and top intersections, consistent with the crack propagation patterns captured during testing. The Gyroid model exhibited better stress distribution and lower deformation levels, confirming its higher stiffness and load-carrying capacity. The Hybrid model displayed minimal stress concentrations and even stress distribution, validating its superior performance under compression.

Assemblage Configuration

Two distinct assemblages were designed to investigate the mechanical performance of TPMS units under compressive loading: the prism assemblage and the diagonal tension assemblage. The prism assemblage (Fig. 2a) consists of three vertically stacked TPMS units, forming a column-like structure with steel plates positioned at the top and bottom surfaces to ensure uniform load distribution. This configuration is intended to simulate the axial compressive behavior of traditional masonry prisms, which enables to evaluate the vertical load-bearing performance and stress transfer mechanisms between units. In contrast, the diagonal tension assemblage (Fig. 1b) comprises nine TPMS units arranged diagonally, with steel plates at the top and bottom to provide boundary constraints and simulate realistic loading conditions. This configuration is designed to model shear-like deformations caused by diagonal tensile stress paths under compression, reflecting scenarios where complex internal force redistributions occur.

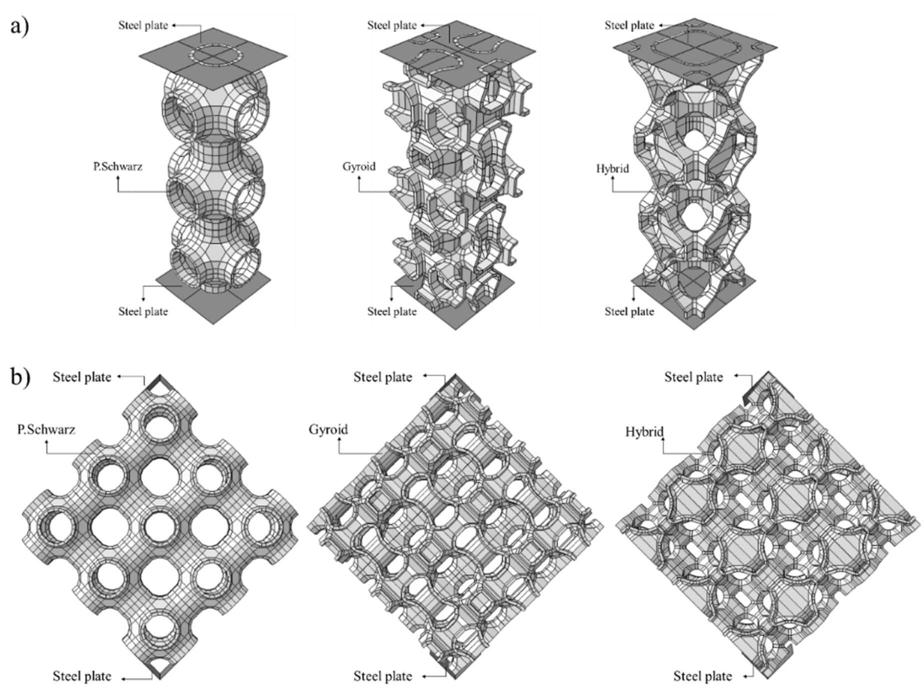

Figure 2: Masonry assemblages: a) Prism and b) Diagonal tension

Detail of Finite Element Modeling

Concrete Damage Plasticity (CDP) model was used to simulate the nonlinear behavior of the TPMS assemblages under compressive loading. The elastic behavior of concrete was defined using an isotropic linear elastic model, while its inelastic response was captured through the CDP model, which is widely recognized for modeling brittle materials like concrete that exhibit brittle failure under tension and quasi-brittle characteristics under compression (Yavartanoo et al., 2024; Afzali et al., 2021; Bolhassani et al., 2015). The model effectively incorporates key failure mechanisms, such as cracking under tensile stress and crushing under compressive loads, while accounting for stiffness degradation through a damage parameter (in tension and compression). The damage variables range from zero, indicating an undamaged material, to one, signifying complete loss of strength. This ensures a realistic simulation of damage accumulation, energy dissipation, and failure progression, making it a suitable choice for evaluating the performance of TPMS assemblages. The material properties used in the models (based on Bolhassani et al., 2015) are summarized in Table 1. For concrete, Young's modulus (E) of 22,600 MPa, density (ρ) of 1.76 × 10^{-9} ton/mm³, and a Poisson's ratio (v) of 0.2 were defined to represent elastic characteristics. The compressive strength (f'_c) of 22.6 MPa and tensile strength (σ) of 2 MPa reflect the mechanical properties required for modeling the brittle behavior of concrete. The CDP model in ABAQUS uses a non-associated plastic flow rule, with the Drucker-Prager hyperbolic function as the flow potential. Key CDP parameters include a dilation angle of 34, which models volumetric expansion under shear stresses, and an eccentricity of 0.1, controlling the yield surface shape and transition between compressive and tensile failure. The biaxial-to-uniaxial compressive strength ratio (f_{bo}/f_{co}) was set to 1.16, capturing confinement effects, while the K parameter, set to 0.67, defines the ratio of secondary stress constants in the tensile and compressive regions, ensuring an accurate representation of stiffness degradation. The damage parameters in both tension and compression were defined as linear functions of inelastic strain in the strain-softening phase.

Table 1: Material Properties

Model	Elastic Material Properties			Concrete Damage Plasticity (CDP) Model					
Concrete	E (MPa)	ρ (ton/mm³)	υ	f'_c (MPa)	σ (MPa)	Dilation Angle	Eccentricity	f_{bo}/f_{co}	K
	22600	1.76 × 10^{-9}	0.2	22.6	2	34	0.1	1.16	0.67

* dilation angle: the angle that expresses the change in the volume of the element under shear stresses;
* f_{bo}/f_{co}: refers to the ratio of the initial biaxial compressive strength to the initial uniaxial compressive strength;
* K: refers to the ratio between the secondary stress constants in the tension and compression regions.

The TPMS units were discretized using C3D10 elements, which are 10-node tetrahedral elements designed for 3D stress analysis. These elements, with quadratic shape functions, effectively capture the curved geometries and stress variations present in the TPMS units, ensuring accurate stress predictions and deformation behavior under compressive loading. The interactions between the concrete TPMS units and the rigid steel plates at the top and bottom surfaces were modeled using tie constraints. These constraints enforce perfect bonding between the components, preventing relative motion or separation at the interfaces. This setup ensures that the applied displacement at the reference point of the top rigid plate is effectively transferred to the TPMS units, replicating realistic load transfer mechanisms observed during experimental tests. Similarly, tie constraints were applied between the TPMS units in the assemblages to maintain mechanical continuity and rigid connections, simplifying the modeling process and accurately representing the behavior of modular structures. The boundary conditions in the finite element (FE) model were carefully designed to replicate the experimental setup used for single TPMS units and extended consistently to the assemblages. Since physical tests were conducted only on single units, their boundary and loading conditions were numerically replicated and applied to the prism and diagonal tension assemblages to ensure comparability between models. Rigid steel plates were modeled at the top and bottom surfaces of both single units and assemblages, with their reference points restrained in all degrees of freedom to prevent translation and rotation. This approach provided uniform load distribution, minimized localized deformations, and accurately simulated compressive loading paths. To apply the compressive load, a displacement-controlled approach was implemented. A vertical displacement was applied at the reference point of the top rigid plate, inducing axial deformation along the vertical axis of the model.

The loading and analysis procedure in the FE model involved a two-step process to accurately simulate the mechanical behavior of the TPMS units and assemblages under compressive loading. In the first step, the self-weight of the structure was applied as a gravity load to the entire model. This step accounted for the effects of gravitational forces on the TPMS units and assemblages, ensuring that the initial stress state due to self-weight was captured before the application of external loads. In the second step, a compressive load was applied by pushing the top rigid plate down using a displacement-controlled approach. The analysis was conducted using a static general solution scheme with nonlinear geometry activated.

RESULTS AND DISCUSSION

The load-displacement curves for the prism and diagonal tension assemblages, constructed using P. Schwarz, Gyroid, and Hybrid units, are shown in Fig. 3. The results highlight the mechanical performance, load-bearing capacities, and failure mechanisms of these assemblages under compressive loading with a maximum displacement of 2 mm.

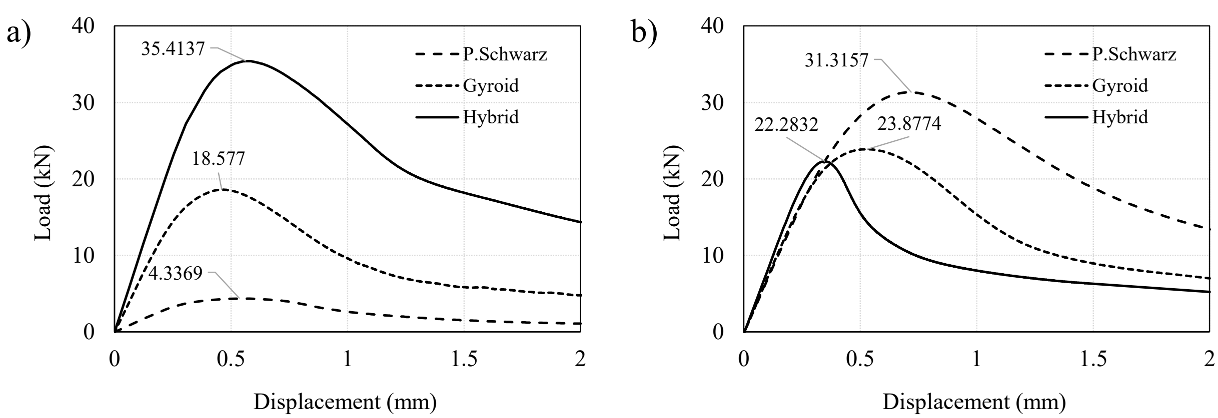

Figure 3: Load-displacement curves: a) Prism and b) Diagonal tension assemblages

In the prism assemblages, the Hybrid model demonstrated the highest load-bearing capacity, reaching a peak load of 35.41 kN. This performance can be attributed to its optimized geometry, which effectively minimizes stress concentrations and provides better load distribution. After reaching the peak load, the Hybrid model exhibited a gradual softening behavior, indicating progressive damage accumulation and higher energy absorption, characteristics desirable for structural applications requiring ductility. The Gyroid model, with a peak load of 18.58 kN, performed moderately compared to the Hybrid model but was 4 times stronger than the P. Schwarz model. Its performance was influenced by its complex geometry, which distributed stresses more efficiently than the P. Schwarz model. However, the Gyroid model experienced a steeper post-peak drop, suggesting more brittle behavior and localized cracking near stress concentration points. In contrast, the P. Schwarz model exhibited the lowest load-bearing capacity, reaching a peak load of only 4.34 kN. Its higher curvature and uneven stress distribution led to localized failures and brittle failure patterns. The rapid drop in load capacity following the peak further emphasizes its limited energy absorption and poor resistance to compressive forces.

In the diagonal tension assemblages, the P. Schwarz model unexpectedly outperformed the other models, reaching a peak load of 31.32 kN. Its curved geometry, which was a limitation under axial compression, proved advantageous in the diagonal configuration, as the stress paths redistributed forces more effectively along the lateral connections. This resulted in a better resistance to shear-induced deformation and delayed failure initiation compared to the other models. The Gyroid model, with a peak load of 22.28 kN, showed better performance than in the prism configuration but still lagged behind the P. Schwarz model. Its intricate geometry allowed for distributed stress transfer, although localized cracks and stress concentrations near the voids led to early damage propagation and brittle failure patterns. The Hybrid model, which excelled under axial compression, showed a lower peak load of 23.88 kN in the diagonal configuration. Although it maintained higher stiffness initially, its geometry was less effective in resisting shear-like deformations, leading to earlier failure and reduced ductility compared to the P. Schwarz model.

The stress distribution and failure mechanisms of the prism assemblages constructed from P. Schwarz, Gyroid, and Hybrid models are illustrated in Fig. 4, showing the maximum principal tensile stress (Fig. 4a) and minimum principal compressive stress (Fig. 4b) at the level of maximum load for each model.

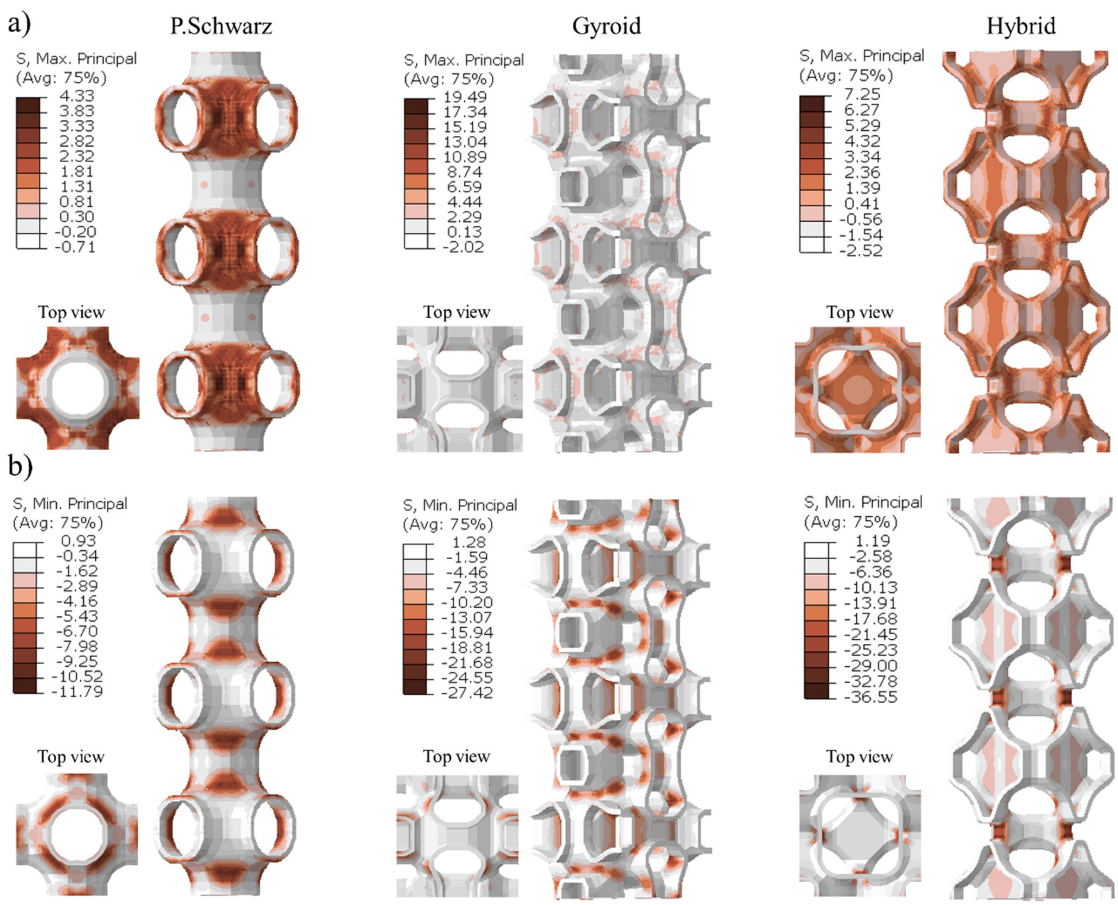

Figure 4: Failure mechanism of prism: a) Tensile and b) Compressive stresses

For the P. Schwarz model, the maximum principal stress indicates that tensile stresses are concentrated around the circular openings and along the vertical connections between the voids. The top view also reveals high stress concentrations at the edges of the openings, where curvature-induced stress amplification occurs. These localized tensile stresses make the P. Schwarz model highly susceptible to cracking at the junctions between voids, consistent with its low load-bearing capacity observed in the load-displacement curves. Similarly, the minimum principal stress distribution shows compressive stress concentrations around the mid-height intersections, which correspond to the regions where failure initiates due to shear and bending effects. In contrast, the Gyroid model exhibits a more distributed stress profile, with tensile stresses concentrated primarily at the sharp edges of its interconnected voids, as shown in the maximum principal stress distribution. Although stress magnitudes are higher compared to the Hybrid model, the Gyroid geometry promotes stress redistribution, reducing the risk of early localized failure. The minimum principal stress map shows compressive stress concentrations near the intersections of the diagonal ribs, indicating regions prone to localized crushing. However, these areas are more evenly distributed than in the P. Schwarz model, contributing to its moderate load-bearing performance and higher energy absorption compared to the P. Schwarz model. The Hybrid model demonstrates the most favorable stress distribution among the three configurations. The maximum principal stress highlights lower tensile stresses compared to the P. Schwarz and Gyroid models, with stress concentrations localized around the central voids and junctions but less pronounced due to its optimized geometry. The minimum principal stress distribution shows compressive stress spread more uniformly along the vertical elements and edges, minimizing localized stress concentrations and enabling the Hybrid model to sustain higher loads without premature failure. Its lower peak tensile stresses and even compressive stress distribution explain its superior performance in the load-displacement curves, highlighting its enhanced structural integrity under compressive forces.

The stress distribution and failure mechanisms of the diagonal tension assemblages are illustrated in Fig. 5, showing the maximum principal tensile stress (Fig. 5a) and minimum principal compressive stress (Fig. 5b).

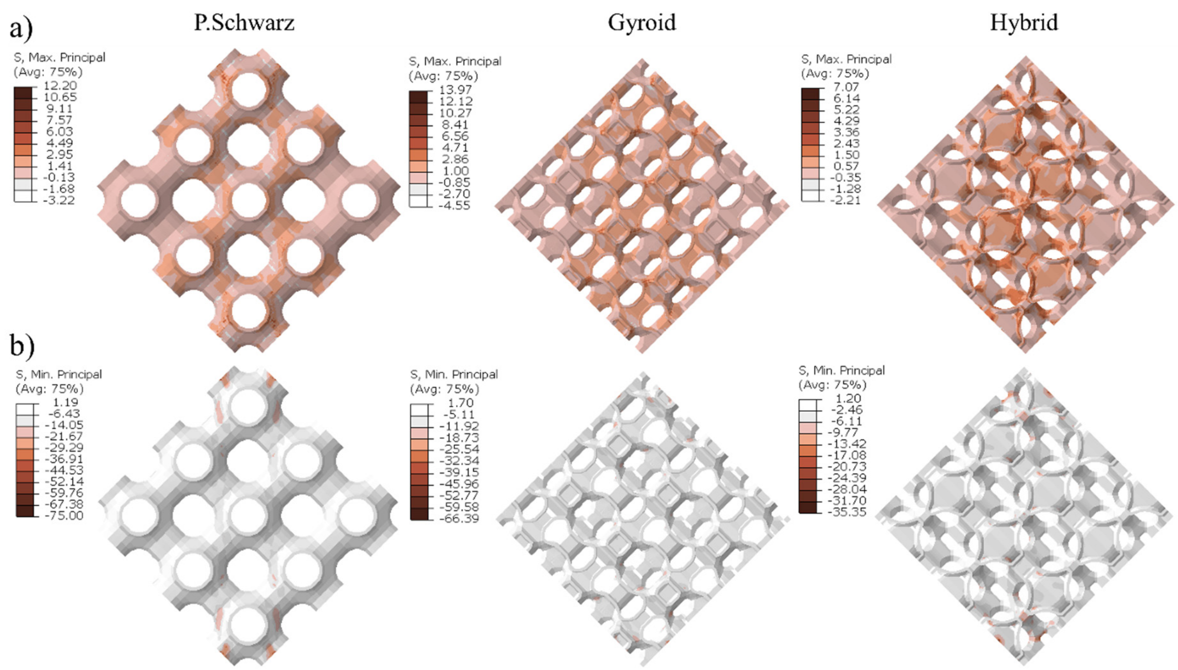

Figure 5: Failure mechanism of diagonal-tension: a) Tensile and b) Compressive stresses

These results highlight the stress patterns, failure modes, and structural behavior of the models under compressive loading applied diagonally. For the P. Schwarz model, the maximum principal stress map (Fig. 4a) reveals that tensile stresses are concentrated around the circular voids and edges, especially at the junctions between connected elements. These areas experience high tensile stress due to bending and flexural actions, leading to localized cracking and tensile failure initiation. The minimum principal stress map (Fig. 5b) indicates that compressive stresses are highly localized around the midpoints of the vertical and diagonal connections, where the geometry promotes stress concentrations. This explains the higher load-carrying capacity observed for the P. Schwarz model in the diagonal configuration, as the stress paths are effectively redistributed through the interconnected arches, delaying failure. However, large compressive stresses near the edges suggest vulnerability to shear-induced cracking, which could propagate under higher loads. The Gyroid model exhibits a more distributed stress profile in both tensile and compressive stress maps. The maximum principal stresses are concentrated at the narrow edges and curved intersections of the voids, reflecting localized stress amplifications caused by the intricate geometry. Despite this, the tensile stresses are generally lower than those observed in the P. Schwarz models, indicating better stress redistribution and delayed crack initiation. The minimum principal stress map highlights areas of high stress concentration around the internal ribs, particularly near void intersections, where localized crushing may occur. However, the ability of Gyroid model to distribute compressive forces across a larger surface area helps reduce premature failure, contributing to its moderate load-bearing performance. The Hybrid model demonstrates the lowest stress concentrations among the three configurations. The maximum principal stress map shows relatively low tensile stresses concentrated around the smaller voids and junctions, reflecting its optimized geometry for reducing stress amplifications. Similarly, the minimum principal stress map reveals a more uniform stress distribution, minimizing localized crushing and enabling better load resistance under diagonal compression. However, compared to the P. Schwarz model, the Hybrid model's geometry appears less effective in redistributing shear forces, leading to lower load capacity despite its superior uniformity under axial loading.

CONCLUSION

This study investigated the numerical behavior of TPMS-based masonry assemblages under compressive loading, focusing on their structural performance, failure mechanisms, and potential applications in modern architectural design. By analyzing prism and diagonal tension assemblages, this research demonstrated the ability of TPMS geometries to optimize stress distribution, reduce localized failures, and enhance load-bearing capacity through their innovative designs. The Hybrid unit emerged as the most effective configuration in the prism assemblages, exhibiting higher load-bearing capacity and optimized stress distribution due to its balanced geometry and reduced stress concentrations. In contrast, the P. Schwarz unit excelled in the diagonal tension assemblages, leveraging its curved geometry to redistribute shear forces more effectively. The Gyroid unit provided moderate performance in both setups, offering a balance between load capacity and stress redistribution but showing localized cracking at stress points. Overall, TPMS-based masonry units demonstrate significant potential for use as sustainable, modular, and structurally efficient architectural elements. Their lightweight nature, material efficiency, and visual appeal make them particularly suitable for non-load-bearing partitions, decorative facades, green walls, and marine structures. This research establishes a foundation for further experimental and computational studies to enhance the design optimization of TPMS systems, enabling their integration into advanced architectural and structural applications.

ACKNOWLEDGEMENTS

This research was conducted at the Advanced Building Construction Lab (ABC Lab) at the Spitzer School of Architecture, The City College of New York. The authors would like to express their gratitude to the Spitzer personnel throughout this study.

REFERENCES

[1] Bolhassani, M., and Wisniewski, S. P. (2022, September). “Design and fabrication of a post-tensioned funicular masonry structure.” In *Proceedings of IASS Annual Symposia*, *12*, 1-10. International Association for Shell and Spatial Structures (IASS).

[2] Nazir, F., Edwards, D. J., Shelbourn, M., Martek, I., Thwala, W. D. D., and El-Gohary, H. (2021). “Comparison of modular and traditional UK housing construction: A bibliometric analysis.” *Journal of Engineering, Design and Technology*, *19*(1), 164-186.

[3] Ferdous, W., Bai, Y., Ngo, T. D., Manalo, A., and Mendis, P. (2019). “New advancements, challenges and opportunities of multi-storey modular buildings–A state-of-the-art review.” *Engineering structures*, *183*, 883-893.

[4] Yavartanoo, F., and Kang, T. H. K. (2022). “Retrofitting of unreinforced masonry structures and considerations for heritage-sensitive constructions.” *Journal of Building Engineering*, *49*, 103993.

[5] Van Mele, T., Lachauer, L., Rippmann, M., & Block, P. (2012). Geometry-based understanding of structures. *Journal of the international association for shell and spatial structures*, *53*(4), 285-295.

[6] Qiu, N., Wan, Y., Shen, Y., & Fang, J. (2024). Experimental and numerical studies on mechanical properties of TPMS structures. *International Journal of Mechanical Sciences*, *261*, 108657.

[7] Feng, J., Fu, J., Yao, X., & He, Y. (2022). Triply periodic minimal surface (TPMS) porous structures: from multi-scale design, precise additive manufacturing to multidisciplinary applications. *International Journal of Extreme Manufacturing*, *4*(2), 022001.

[8] Meza, L. R., Das, S., & Greer, J. R. (2014). Strong, lightweight, and recoverable three-dimensional ceramic nanolattices. *Science*, *345*(6202), 1322-1326.

[9] Nguyen-Van, V., Tran, P., Peng, C., Pham, L., Zhang, G., & Nguyen-Xuan, H. (2020). Bioinspired cellular cementitious structures for prefabricated construction: Hybrid design & performance evaluations. *Automation in Construction*, *119*, 103324.

[10] Sokollu, B., Gulcan, O., & Konukseven, E. I. (2022). Mechanical properties comparison of strut-based and triply periodic minimal surface lattice structures produced by electron beam melting. *Additive Manufacturing*, *60*, 103199.

[11] Yoris-Nobile, A. I., Slebi-Acevedo, C. J., Lizasoain-Arteaga, E., Indacoechea-Vega, I., Blanco-Fernandez, E., Castro-Fresno, D., ... & Lobo-Arteaga, J. (2023). Artificial reefs built by 3D printing: Systematisation in the design, material selection and fabrication. *Construction and Building Materials*, *362*, 129766.

[12] Hooshmand-Ahoor, Z., Luo, H., & Danas, K. (2024). M-Voronoi and other random open and closed-cell elasto-plastic cellular materials: Geometry generation and numerical study at small and large strains. *International Journal of Solids and Structures*, *290*, 112680.

[13] Gide, K. M., & Bagheri, Z. S. (2024). Mechanical behavior and material modeling of fused filament fabricated PEEK based on TPMS lattices: a comparative study. *The International Journal of Advanced Manufacturing Technology*, *134*(5), 2765-2780.

[14] Righi, M., Yavartanoo, F., Alaeva, S., & Bolhassani, D. (2024). Design, fabrication and analysis of triply periodic minimal surface concrete units. *Journal of Building Engineering*, *98*, 111286.

[15] Yavartanoo, F., Kim, T., Kim, J., Jang, H., & Kim, C. S. (2024). Out-of-plane behavior of U-shaped unreinforced masonry structures. *Journal of Building Engineering*, *86*, 108984.

[16] Afzali, S., Alinejad, H., Nasrollahzadeh, K., & Kang, T. H. K. (2021). Modeling of Near-Surface-Mounted Fiber-Reinforced Polymer Strips to Concrete. *ACI Structural Journal*, *118*(5).

[17] Bolhassani, M., Hamid, A. A., Lau, A. C., & Moon, F. (2015). Simplified micro modeling of partially grouted masonry assemblages. *Construction and Building Materials*, *83*, 159-173.